

Article

Thermoelectric Generator Using Polyaniline-Coated $\text{Sb}_2\text{Se}_3/\beta\text{-Cu}_2\text{Se}$ Flexible Thermoelectric Films

Minsu Kim ¹, Dabin Park ¹ and Jooheon Kim ^{1,2,*} 

¹ School of Chemical Engineering & Materials Science, Chung-Ang University, Seoul 06974, Korea; alstn275@gmail.com (M.K.); dragoo@naver.com (D.P.)

² Department of Advanced Materials Engineering, Chung-Ang University, Anseong-si, Seoul 17546, Korea

* Correspondence: jooheonkim@cau.ac.kr

Abstract: Herein, Sb_2Se_3 and $\beta\text{-Cu}_2\text{Se}$ nanowires are synthesized via hydrothermal reaction and water evaporation-induced self-assembly methods, respectively. The successful syntheses and morphologies of the Sb_2Se_3 and $\beta\text{-Cu}_2\text{Se}$ nanowires are confirmed via X-ray powder diffraction (XRD), X-ray photoelectron spectroscopy (XPS), Raman spectroscopy, field emission scanning electron microscopy (FE-SEM), and field emission transmission electron microscopy (FE-TEM). Sb_2Se_3 materials have low electrical conductivity which limits application to the thermoelectric generator. To improve the electrical conductivity of the Sb_2Se_3 and $\beta\text{-Cu}_2\text{Se}$ nanowires, polyaniline (PANI) is coated onto the surface and confirmed via Fourier-transform infrared spectroscopy (FT-IR), FE-TEM, and XPS analysis. After coating PANI, the electrical conductivities of $\text{Sb}_2\text{Se}_3/\beta\text{-Cu}_2\text{Se}/\text{PANI}$ composites were increased. The thermoelectric performance of the flexible $\text{Sb}_2\text{Se}_3/\beta\text{-Cu}_2\text{Se}/\text{PANI}$ films is then measured, and the 70%- $\text{Sb}_2\text{Se}_3/30\%\text{-}\beta\text{-Cu}_2\text{Se}/\text{PANI}$ film is shown to provide the highest power factor of $181.61 \mu\text{W}/\text{m}\cdot\text{K}^2$ at 473 K. In addition, a thermoelectric generator consisting of five legs of the 70%- $\text{Sb}_2\text{Se}_3/30\%\text{-}\beta\text{-Cu}_2\text{Se}/\text{PANI}$ film is constructed and shown to provide an open-circuit voltage of 7.9 mV and an output power of 80.1 nW at $\Delta T = 30$ K. This study demonstrates that the combination of inorganic thermoelectric materials and flexible polymers can generate power in wearable or portable devices.

Keywords: antimony selenide; copper selenide; polyaniline; thermoelectric generator



Citation: Kim, M.; Park, D.; Kim, J. Thermoelectric Generator Using Polyaniline-Coated $\text{Sb}_2\text{Se}_3/\beta\text{-Cu}_2\text{Se}$ Flexible Thermoelectric Films.

Polymers **2021**, *13*, 1518. <https://doi.org/10.3390/polym13091518>

Academic Editor: Mohammad Arjmand

Received: 11 April 2021

Accepted: 3 May 2021

Published: 9 May 2021

Publisher's Note: MDPI stays neutral with regard to jurisdictional claims in published maps and institutional affiliations.



Copyright: © 2021 by the authors. Licensee MDPI, Basel, Switzerland. This article is an open access article distributed under the terms and conditions of the Creative Commons Attribution (CC BY) license (<https://creativecommons.org/licenses/by/4.0/>).

1. Introduction

In recent years, thermoelectric materials have been studied for use in the thermoelectric generator (TEG) or Peltier cooler. In particular, inorganic thermoelectric materials based on Bi_2Te_3 [1,2], PbTe [3,4], SnSe [5,6], Cu_2Se [7,8], skutterudites [9,10], and Zintl phases [11,12] have been studied during the past few decades. Although such inorganic thermoelectric materials exhibit better performance than their organic counterparts, they are difficult to use in wearable or portable devices due to their rigid (inflexible), brittle, heavy, costly, and toxic properties. Conversely, organic thermoelectric materials such as the conducting polymers PEDOT:PSS [13–15], polyaniline (PANI) [16–18], polythiophene [19], and polypyrrole [20,21] can exhibit lightweight, low-cost, non-toxic, and flexible properties but display low efficiency compared to their inorganic counterparts. To overcome these difficulties associated with using inorganic or organic thermoelectric materials alone, hybrid inorganic/organic thermoelectric materials have been studied in the most recent decades. In addition, the electrical conductivities of various hybrid materials have been further improved by various coating methods. For example, C. Meng et al. reported a promising improvement in the thermoelectric performance of carbon nanotubes up to 4–5 times by enwrapping the base material in PANI to provide a size-dependent energy-filtering effect [17]. In addition, D. Park et al. reported enhanced thermoelectric properties using Ag_2Se nanowire/Polyvinylidene fluoride composite film via a solution mixing method.

These studies show a combination of inorganic thermoelectric materials and polymers can be used for improvement thermoelectric performances [22].

Antimony selenide (Sb_2Se_3) is a chalcogenide material that is easy to synthesize in various structures such as thin films [23], nanosheets [24], and nanorods/wires [25,26]. Although Sb_2Se_3 has a large Seebeck coefficient of $750 \mu\text{V}/\text{K}$, the extremely low electrical conductivity of $10^{-4} \text{ S}/\text{m}$ [26] is a limitation in thermoelectric applications. To address this problem, an alloy of Sb_2Se_3 with copper selenide (Cu_2Se) is proposed herein. Also a chalcogenide, Cu_2Se complements Sb_2Se_3 by exhibiting a high electrical conductivity along with a low Seebeck coefficient. Similarly to Sb_2Se_3 , Cu_2Se is easy to synthesize in various structures, including films [13], nanoplates [27], and nanowires [28]. In our previous work, $\beta\text{-Cu}_2\text{Se}$ nanowires were synthesized and combined with Sb_2Se_3 nanowires to make the rigid disk shape composite to improve thermoelectric performance [29]. In addition to our previous work, to further improve the electrical conductivity of the $\text{Sb}_2\text{Se}_3/\beta\text{-Cu}_2\text{Se}$ composite, the conducting polymer polyaniline (PANI) (with an electrical conductivity of $360 \text{ S}/\text{cm}$ [16]) was used to coat the composite surface. Moreover, in our previous work, it was found that the rigid and brittle nature of the resulting inorganic thermoelectric composites makes them difficult to use in preparing flexible films. To address this problem, a flexible thin film of polyvinylidene fluoride (PVDF) is developed. The flexible thin film with 70% $\beta\text{-Cu}_2\text{Se}$ and 30% Sb_2Se_3 nanowires is shown to provide a power factor of $181.61 \mu\text{W}/\text{m}\cdot\text{K}^2$. This film is then used to fabricate a thermoelectric device with an output voltage of 7.9 mV and an output power of 80.1 nW at a temperature difference of 30 K. These results demonstrate that the $\text{Sb}_2\text{Se}_3/\beta\text{-Cu}_2\text{Se}/\text{PANI}$ flexible thin film can be used as a TEG for flexible devices.

2. Experimental Section

2.1. Materials

Sodium selenite (Na_2SeO_3 , 99.9%), selenium powder (Se, 99.5%), and sodium dodecylbenzene sulfonate ($\text{CH}_3(\text{CH}_2)_{11}\text{C}_6\text{H}_4\text{SO}_3\text{Na}$, SDBS) were purchased from Sigma-Aldrich. Potassium antimony tartrate ($\text{C}_8\text{H}_4\text{K}_2\text{O}_{12}\text{Sb}_2\cdot 3\text{H}_2\text{O}$, 99.5) was acquired from FUJIFILM Wako Pure Chemical Corporation (Osaka, Japan). Ammonium peroxydisulfate ($(\text{NH}_4)_2\text{S}_2\text{O}_8$, APS, 98%) was purchased from Alfa Aesar. Sodium hydroxide (NaOH, 97%), copper(II) nitrate trihydrate ($\text{Cu}(\text{NO}_3)_2\cdot 3\text{H}_2\text{O}$, 99%), hydrazine monohydrate ($\text{N}_2\text{H}_4\cdot \text{H}_2\text{O}$, 80%), tetrahydrofuran ($(\text{CH}_2)_4\text{O}$, 99%), m-cresol ($\text{C}_7\text{H}_8\text{O}$, 98%), D(+)-10-camphorsulfonic acid ($\text{C}_{10}\text{H}_{16}\text{O}_4\text{S}$, CSA, 98%), Dimethylformamide ($\text{C}_3\text{H}_7\text{NO}$, DMF), and aniline ($\text{C}_6\text{H}_5\text{NH}_2$, 99%) were acquired from Daejung Chemical and Metals Co., Ltd. (Seoul, Korea). All reagents were used as received without further purification.

2.2. Sample Preparation

2.2.1. Synthesis of Sb_2Se_3 Nanowires

The selenium and antimony precursors were reduced using hydrazine monohydrate and synthesized to Sb_2Se_3 nanowires using a previously reported method [24]. In detail, potassium antimony tartrate (0.605 g) and sodium selenite (0.51 g) were completely dissolved in distilled water (100 mL) with magnetic stirring. Hydrazine monohydrate (30 mL) was then added, and the mixture was transferred to a Teflon-lined autoclave with tetrahydrofuran (40 mL). The sealed autoclave was heated to $135 \text{ }^\circ\text{C}$ for 9 h, then the product was centrifuged at 10,000 rpm for 1 h, washed several times with distilled water and ethanol, then dried overnight in a vacuum oven at $70 \text{ }^\circ\text{C}$.

2.2.2. Synthesis of $\beta\text{-Cu}_2\text{Se}$ Nanowires

The $\beta\text{-Cu}_2\text{Se}$ nanowires were synthesized via a previously reported method [28]. In detail, a mixture of Se powder (0.45 g) and NaOH (15 g) in distilled water (60 mL) was heated at $90 \text{ }^\circ\text{C}$ to completely dissolve the Se powder. Then, a 0.5 M $\text{Cu}(\text{NO}_3)_2$ solution (5 mL) was added, and the mixture was heated to dryness in an oven at $140 \text{ }^\circ\text{C}$ for 12 h.

The precipitated product was then collected using hot distilled water, washed several times with hot distilled water and ethanol, then dried overnight in a vacuum oven at 60 °C.

2.2.3. Synthesis of Sb₂Se₃/β-Cu₂Se/PANI Composite Films and Fabrication of a TEG Device

The SDBS (0.06 g) was dissolved in 1 M HCl solution (10 mL), followed by sonication for 30 min to prepare a homogeneous solution. Using an ice bath to maintain a temperature of 273 K, the aniline monomer (0.02 g) was then added to the solution with steady stirring for 12 h. Then, APS (0.04 g) was dissolved in HCl solution (5 mL) and slowly added to the prepared solution. The product was then washed three times with distilled water and dried overnight in a vacuum oven at 60 °C to obtain the polyaniline powder.

Using the same polymerization procedure, Sb₂Se₃/β-Cu₂Se/PANI powders were synthesized by adding various ratios of Sb₂Se₃ and β-Cu₂Se to 1 M HCl solution (10 mL), SDBS (0.06 g), and aniline monomer (0.02 g). The obtained Sb₂Se₃/β-Cu₂Se/PANI powders were then added to 1 M ammonia solution (10 mL) and magnetically stirred for 24 h to prepare the emeraldine base PANI product. The products were then washed several times with distilled water and dried overnight in a vacuum oven at 60 °C. To improve the electrical conductivity of the emeraldine base PANI, CSA was used as a dopant in *m*-cresol (10 mL) in a mole ratio of 1:2 with stirring for 24 h. The obtained powder was dried overnight in a vacuum oven at 60 °C.

To synthesize the Sb₂Se₃/β-Cu₂Se/PANI film, the Sb₂Se₃/β-Cu₂Se/PANI powder (0.05 g) and polyvinylidene fluoride (PVDF) (0.025 g) were added to DMF solution (1 mL) at a weight ratio of 2:1 and sonicated for 1h to generate a homogenous mixture. The mixture was then drop-casted onto a glass substrate (18 mm × 18 mm) and dried at 60 °C for 24 h.

To fabricate a TEG device, the Sb₂Se₃/β-Cu₂Se/PANI film was cut into five (18 mm × 6 mm) strips with a thickness of 100 μm. These were then pasted onto a polyimide film and connected with copper wire. Silver (Ag) adhesive (ELCOAT P-100, CANS) was used to connect the copper wire and film.

2.3. Characterization

The crystalline structures of the prepared nanowire powders and de-doped PANI were examined by X-ray diffraction (XRD; D8 Advance, AXS Bruker, Billerica, US) under Cu K_α radiation ($\lambda = 0.154056$ nm) at 40 kV and 40 mA over a 2 θ range of 10–80° at a scan rate of 1° s⁻¹. The binding energies of the synthesized nanowires and Sb₂Se₃/β-Cu₂Se/PANI powders were determined via X-ray photoelectron spectroscopy (XPS; K-Alpha, Thermo Fisher Scientific, Waltham, USA) using a 1486.6 eV Al K_α X-ray source. Fourier-transform infrared (FT-IR) spectroscopy (PerkinElmer Spectrum One) was conducted to confirm the synthesis of PANI. Raman spectra were recorded using a Raman spectrometer II (DXR2xi, Thermo Fisher Scientific, Waltham, USA) with a near infrared laser operating at 532 nm and a CCD detector. Field emission scanning electron microscopy (FE-SEM; SIGMA, Oberkochen, Germany), and field emission transmission electron microscopy (FE-TEM; JEM-F200) were used to visualize the shape and microstructures of the Sb₂Se₃ and Cu₂Se nanowire samples. Energy-dispersive X-ray spectroscopy (EDS) was used to obtain the elemental mappings of the nanowire powders (JEM-F200, JEOL Ltd., Akishima, Japan). The thermoelectric properties, Seebeck coefficients, and electrical conductivities were measured in the direction parallel to the pressing direction. A four-probe method involving a homemade device with a pair of thermocouples and a pair of voltmeters was used to quantify the electrical conductivity (σ) between room temperature (RT) and 473 K, and the Seebeck coefficient was calculated from the relationship in Equation (1):

$$S = \Delta V / \Delta T \quad (1)$$

where ΔV is the change in the thermal electromotive force and ΔT is the temperature difference.

In addition, the power factor (PF) was calculated using Equation (2):

$$PF = S^2 \cdot \sigma \quad (2)$$

The properties of the generator were measured using a homemade device with thermocouples and a multimeter (SENIT, A830L).

3. Results and Discussion

3.1. Crystallin Structure and Morphology of Sb_2Se_3 Nanowires

The Sb_2Se_3 nanowires with diameters of 100–200 nm and lengths of 1–2 μm were successfully synthesized via the hydrothermal reaction, as shown in Figure 1a.

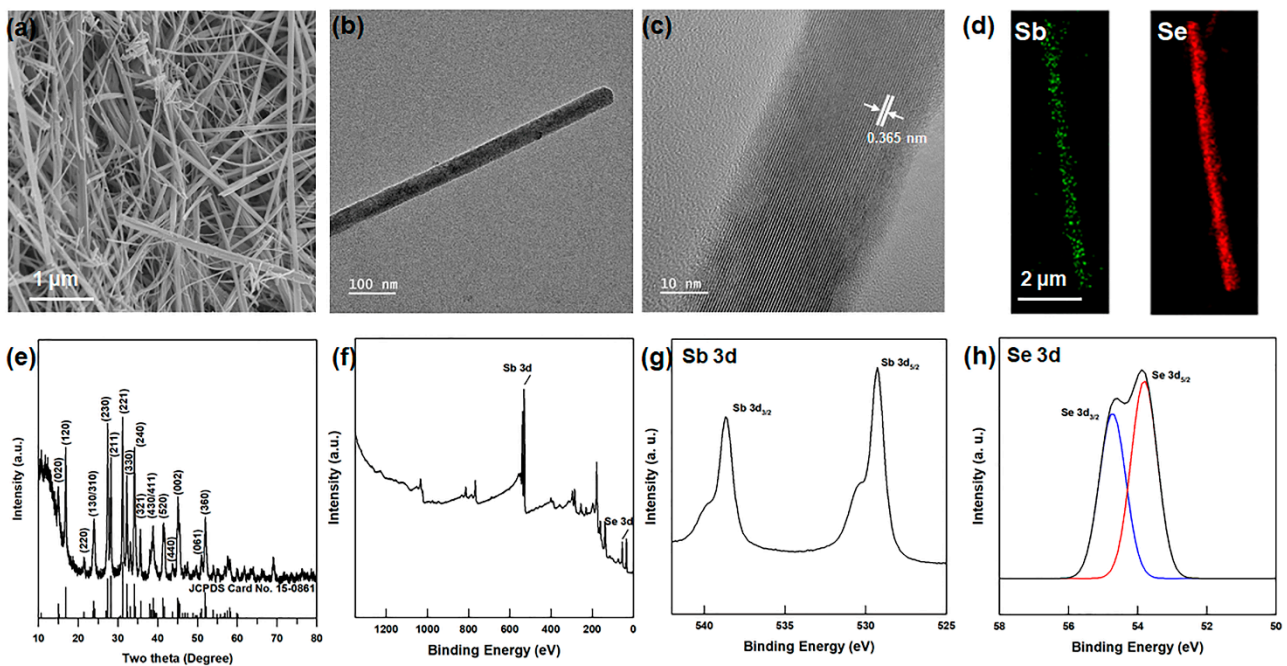


Figure 1. (a) FE-SEM image (b) FE-TEM (c) high-resolution of FE-TEM images of Sb_2Se_3 nanowires. EDS elemental mapping of (d) Sb and Se in Sb_2Se_3 nanowires. (e) XRD patterns and (f) XPS survey spectrum of Sb_2Se_3 nanowires. High-resolution XPS spectra of (g) Sb 3d peaks and (h) Se 3d peaks in Sb_2Se_3 nanowires.

In addition, the FE-TEM images of the Sb_2Se_3 nanowires are presented in Figure 1b,c. Here, the lattice fringes of the Sb_2Se_3 nanowires are 0.365 nm in size, which corresponds to the (1 3 0) crystal plane [30]. The EDS mappings of the Sb_2Se_3 nanowires in Figure 1d,e indicate a stoichiometric atomic ratio of Sb:Se = 42.01:57.99. Moreover, the XRD pattern of the Sb_2Se_3 nanowires in Figure 1f reveals a diffraction peak with lattice constants of $a = 1.168$ nm, $b = 1.172$ nm, and $c = 0.397$ nm, corresponding to the orthorhombic structure (JCPDS #15-0681, $a = 1.1633$ nm, $b = 1.1780$ nm, and $c = 0.3985$ nm). The absence of any second phase peaks demonstrates the high purity of the nanowires, and the strong intensities of the (h k 0) planes indicate that the Sb_2Se_3 particles have a 1-dimensional nanowire structure. Further, the XPS spectra of the Sb_2Se_3 nanowires are presented in Figure 1g–i. Here, the XPS wide scan spectra exhibit the Sb 3d and Se 3d peaks with no O 1s peak, thus indicating that the Sb_2O_3 phase was not produced during the synthesis, in agreement with the above interpretation of the XRD pattern. Further, the high-resolution Sb 3d spectrum in Figure 1h exhibits the Sb 3d_{5/2} and Sb 3d_{3/2} peaks at binding energies of 529.5 and 538.8 eV, respectively, in agreement with the previously reported data [24]. Similarly, the binding energies of Se 3d_{5/2} and Se 3d_{3/2} are located at 53.91 and 54.73 eV, which is in close agreement with the previously reported data [25]. The atomic ratio of Sb:Se obtained from the XPS spectra is 41.21:58.79, which is close to that obtained from

the EDS mapping data and to the stoichiometric ratio. The Raman spectrum of the Sb_2Se_3 nanowires is provided in Figure S1 of the Supplementary Information. Here, the peaks located at 118, 188, and 208 cm^{-1} are consistent with the Sb_2Se_3 phase [31,32], whereas the peak at 252 cm^{-1} is consistent with the Sb_2O_3 phase. As this second phase was not observed in the XRD pattern and XPS spectra, the small Raman peak can be attributed to oxidation of the Sb_2Se_3 surface to Sb_2O_3 by the high-density laser ($1\text{ mW}/\mu\text{m}^2$) of the Raman II instrument [31].

3.2. Crystallin Structure and Morphology of $\beta\text{-Cu}_2\text{Se}$ Nanowires

The $\beta\text{-Cu}_2\text{Se}$ nanowires with diameters of 100–200 nm diameter and lengths of 1–2 μm were obtained as shown in Figure 2a.

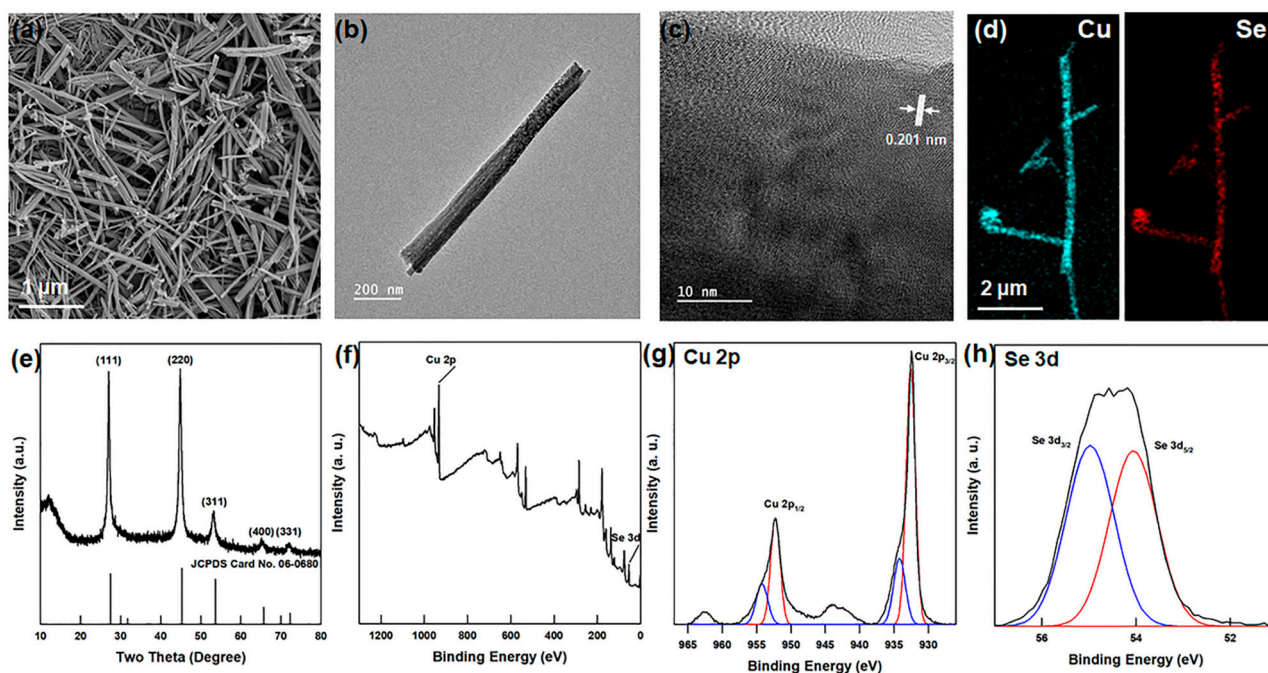


Figure 2. (a) FE-SEM image (b) FE-TEM (c) high-resolution of FE-TEM images of $\beta\text{-Cu}_2\text{Se}$ nanowires. EDS elemental mapping of (d) Cu and Se in $\beta\text{-Cu}_2\text{Se}$ nanowires. (e) XRD patterns and (f) XPS survey spectrum of $\beta\text{-Cu}_2\text{Se}$ nanowires. High-resolution XPS spectra of (g) Cu 2p peaks and (h) Se 3d peaks in $\beta\text{-Cu}_2\text{Se}$ nanowires.

Further, the FE-TEM images in Figure 2b,c exhibit 0.201 nm lattice fringes corresponding to the (2 2 0) crystal plane. In addition, the EDS mapping images in Figure 2d,e indicate an atomic ratio of Cu:Se = 68.14:31.86, which is close to the stoichiometric ratio. Meanwhile, the XRD pattern of $\beta\text{-Cu}_2\text{Se}$ in Figure 2f exhibits a diffraction peak with a lattice constant of $a = 0.5692\text{ nm}$, corresponding to the cubic structure (JCPDS #06-0680, $a = 0.5759\text{ nm}$). The absence of any peaks of the second phases in the XRD pattern corresponding to other phases indicates the high purity of the $\beta\text{-Cu}_2\text{Se}$ nanowires.

For further characterization, the XPS spectra of the $\beta\text{-Cu}_2\text{Se}$ nanowires are presented in Figure 2g,i. Here, the presence of the Cu^+ oxidation state is indicated by the Cu $2p_{3/2}$ and Cu $2p_{1/2}$ peaks located at binding energies of 933.66 and 954.56 eV, respectively (Figure 2h). The relatively weaker peaks at 932.38 and 952.33 eV indicate the presence of the Cu^{2+} oxidation state, but other phases such as CuO are not observed. In addition, the Se $3d_{5/2}$ and Se $3d_{3/2}$ peaks are located at binding energies of 54.01 and 54.94 eV, respectively (Figure 2i). Further, the atomic ratio of Cu:Se is seen to be 64.76:35.24, which is in agreement with that obtained from the EDS mapping ratio and with the stoichiometric ratio. The Raman spectrum of the $\beta\text{-Cu}_2\text{Se}$ nanowire is provided in Figure S2. Here, the peak at 260 cm^{-1} corresponds to the previously reported Raman data for $\beta\text{-Cu}_2\text{Se}$ [33]. In contrast to the Raman spectrum of the Sb_2Se_3 nanowires (Figure S1), no oxidized peak

is observed for the β -Cu₂Se nanowires. This confirms the high purity of the synthesized β -Cu₂Se nanowires.

3.3. Confirmation of PANI Coated Sb₂Se₃/ β -Cu₂Se Nanowire Powders

The XRD pattern of the de-doped PANI is presented in Figure 3a and is in agreement with the previously reported data [34].

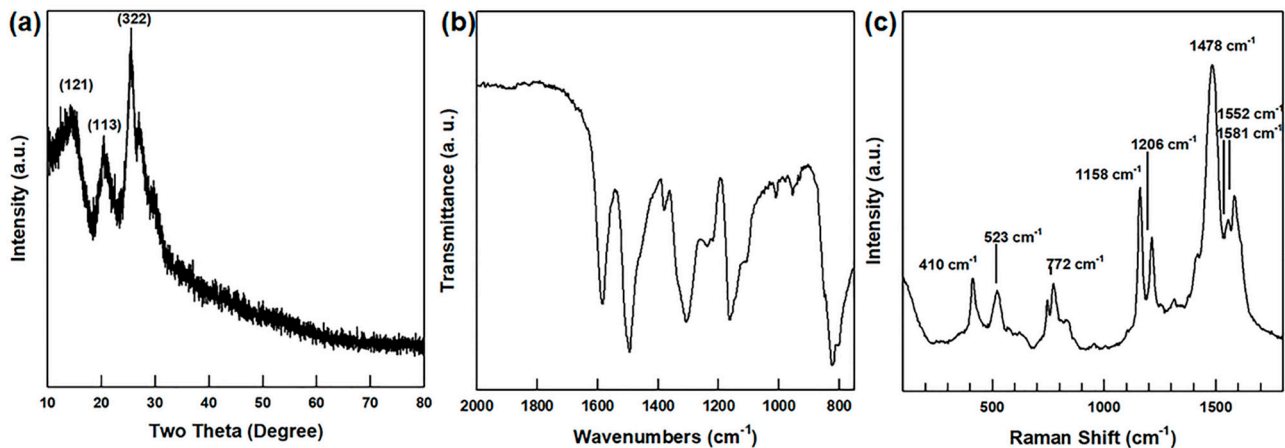


Figure 3. (a) XRD patterns, (b) FT-IR spectrum, and (c) Raman spectrum of de-doped PANI powder.

In addition, the FT-IR spectrum of the de-doped PANI is presented in Figure 3b. Here, the peaks at 1587 and 1490 cm^{-1} are attributed to the C=C stretching vibrations of the quinoid and benzenoid ring, respectively; the peaks at 1300 and 1240 cm^{-1} indicate the C-N stretching of the benzenoid ring, and the peak at 1151 cm^{-1} indicates the N=quinoid-ring=N vibrational mode [35]. Taken together, the FT-IR and XRD results demonstrate the successful synthesis of the de-doped PANI with the emeraldine structure incorporating both the benzenoid and quinoid rings.

By comparison, the FT-IR spectrum of the composite Sb₂Se₃/ β -Cu₂Se/PANI material in Figure 4a reveals the appearance of peaks at 1591, 1490, 1300, 1240, and 1151 cm^{-1} due to the PANI coated on the surface of Sb₂Se₃ and β -Cu₂Se nanowires.

Further, the FE-SEM images of the composite materials with various ratios of Sb₂Se₃ and β -Cu₂Se nanowires in Figure S3 reveal the change in morphology and increased roughness of the Sb₂Se₃/ β -Cu₂Se/PANI nanowire surface. In addition, the FE-TEM images in Figure 4b–f indicate that the PANI is coated on the surface of the Sb₂Se₃/ β -Cu₂Se nanowires with a uniform thickness of 4–5 nm. For further characterization, the N 1s and C 1s peaks in the XPS spectra of the 70%-Sb₂Se₃/30%- β -Cu₂Se/PANI composites are presented in Figure 4g,h. Here, the peaks at 398.15, 400.04, and 402.25 eV are respectively attributed to the –N= bonds, the –NH– bonds, and the N⁺ species of the emeraldine base PANI [36]. Meanwhile, the binding energies of 284.38 and 286.31 eV are attributed to the C–C/C–H bonds and the C–N bonds, respectively, of the emeraldine based PANI [36]. Taken together, the FE-TEM and XPS results demonstrate the successful formation of PANI on the surface of the nanowires.

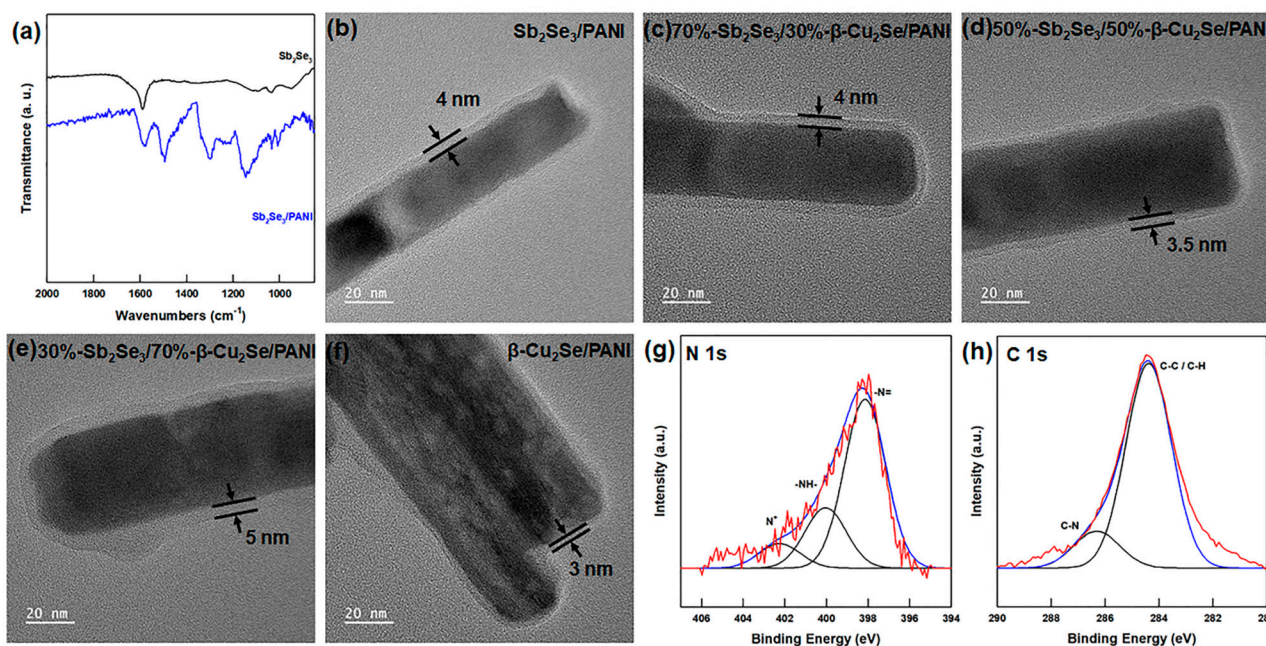


Figure 4. (a) FT-IR spectrum of Sb_2Se_3 nanowires and $\text{Sb}_2\text{Se}_3/\text{PANI}$ powder. High-resolution FE-TEM images of (b) $\text{Sb}_2\text{Se}_3/\text{PANI}$, (c) 70%- $\text{Sb}_2\text{Se}_3/30\%-\beta\text{-Cu}_2\text{Se}/\text{PANI}$, (d) 50%- $\text{Sb}_2\text{Se}_3/50\%-\beta\text{-Cu}_2\text{Se}/\text{PANI}$, (e) 30%- $\text{Sb}_2\text{Se}_3/70\%-\beta\text{-Cu}_2\text{Se}/\text{PANI}$, and (f) $\beta\text{-Cu}_2\text{Se}/\text{PANI}$ powders. High-resolution XPS spectra of (g) N 1s peaks and (h) C 1s peaks in 70%- $\text{Sb}_2\text{Se}_3/30\%-\beta\text{-Cu}_2\text{Se}/\text{PANI}$ powders.

3.4. Thermoelectric Properties of $\text{Sb}_2\text{Se}_3/\beta\text{-Cu}_2\text{Se}/\text{PANI}$ Flexible Films and TEG Properties

The $\text{Sb}_2\text{Se}_3/\beta\text{-Cu}_2\text{Se}/\text{PANI}$ films were synthesized from the $\text{Sb}_2\text{Se}_3/\beta\text{-Cu}_2\text{Se}/\text{PANI}$ powders with various ratios of Sb_2Se_3 and $\beta\text{-Cu}_2\text{Se}$ as described in Section 2.2.3. The flexible properties of the obtained films are indicated in Figure S4, while the Seebeck coefficients (S) and electrical conductivities (σ) of the $\text{Sb}_2\text{Se}_3/\beta\text{-Cu}_2\text{Se}$ nanowires and $\text{Sb}_2\text{Se}_3/\beta\text{-Cu}_2\text{Se}/\text{PANI}$ films are indicated in Figure 5a,b.

Here, the pure Sb_2Se_3 and $\beta\text{-Cu}_2\text{Se}$ exhibit Seebeck coefficients of 400 and 3–4 $\mu\text{V}/\text{K}$, respectively, while the Seebeck coefficient of the $\text{Sb}_2\text{Se}_3/\beta\text{-Cu}_2\text{Se}$ composite is seen to decrease with increasing proportion of $\beta\text{-Cu}_2\text{Se}$. Meanwhile, the electrical conductivity of the $\text{Sb}_2\text{Se}_3/\beta\text{-Cu}_2\text{Se}$ composites is seen to increase with the increasing proportion of $\beta\text{-Cu}_2\text{Se}$ due to the high electrical conductivity of $\beta\text{-Cu}_2\text{Se}$ (45.3 S/cm^{-1}). Compared to the non-coated $\text{Sb}_2\text{Se}_3/\beta\text{-Cu}_2\text{Se}$ composite, the $\text{Sb}_2\text{Se}_3/\beta\text{-Cu}_2\text{Se}/\text{PANI}$ film exhibits a lower Seebeck coefficient and a higher electrical conductivity due to the high electrical conductivity of PANI (i.e., 360 S/cm) [16]. These trends in the Seebeck coefficient and electrical conductivity can be explained by a parallel-connected model, as described in the Supporting Information. Although the complicated interfacial interactions can distort the electrical conductivity curves and, thus, lead to inaccuracy, the parallel-connected model can be considered a useful guideline [37–39]. The results of the parallel-connected model are indicated by the dashed line in Figure 5a,b, while the Seebeck coefficients, electrical conductivities, and power factors of the $\text{Sb}_2\text{Se}_3/\beta\text{-Cu}_2\text{Se}$ nanowires and $\text{Sb}_2\text{Se}_3/\beta\text{-Cu}_2\text{Se}/\text{PANI}$ films over the temperature range of room temperature to 473 K are presented in Figure 5c–e.

In all cases, the Seebeck coefficients and electrical conductivities are seen to increase with the increasing temperature. In addition, the maximum power factor (PF), as calculated using Equation (2), is 181.61 $\mu\text{W}/\text{m}\cdot\text{K}^2$ for the 70%- $\text{Sb}_2\text{Se}_3/30\%-\beta\text{-Cu}_2\text{Se}/\text{PANI}$ film.

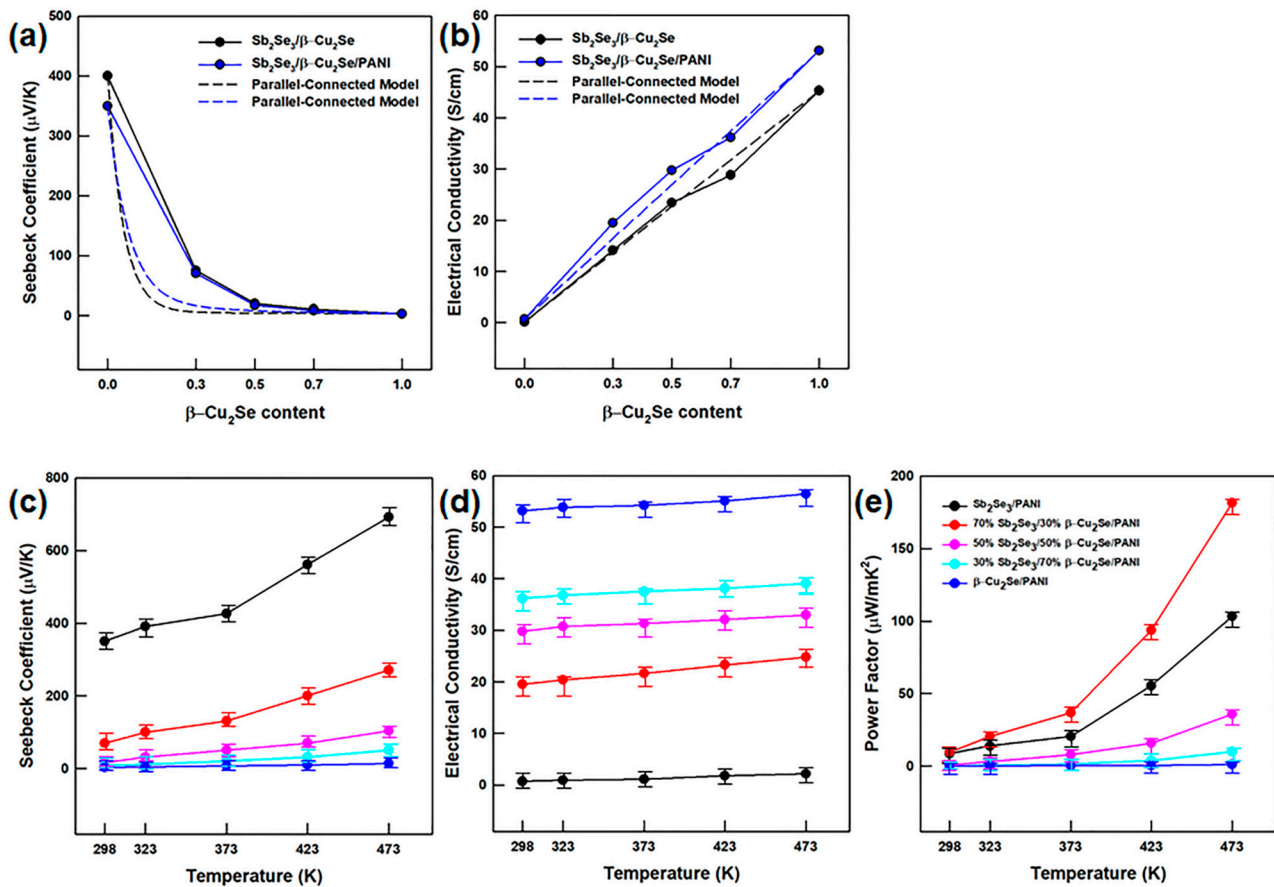


Figure 5. β - Cu_2Se -ratio-dependent (a) Seebeck coefficients and (b) electrical conductivities of various ratios of $\text{Sb}_2\text{Se}_3/\beta\text{-Cu}_2\text{Se}/\text{PANI}$ films at room temperature. Temperature-dependent (c) Seebeck coefficients, (d) electrical conductivities, and (e) power factors of various ratios of $\text{Sb}_2\text{Se}_3/\beta\text{-Cu}_2\text{Se}/\text{PANI}$ films.

The flexible film of thermoelectric materials can be used as a TEG for wearable or portable devices. Hence, the highest-performing material in the present study, namely the 70%- $\text{Sb}_2\text{Se}_3/30\%\beta\text{-Cu}_2\text{Se}/\text{PANI}$ film, was used to fabricate a TEG, as shown in Figure 6a. The open-circuit voltage (V_{oc}) and output power of the device are indicated in Figure 6b,c. The open-circuit voltage of the fabricated TEG was measured under a temperature difference of $\Delta T = 30$ K and reached a value of 7.9 mV. The theoretical value of the open-circuit voltage was calculated using Equation (3):

$$V_{oc} = N \cdot |S| \cdot \Delta T \quad (3)$$

where N is the number of TEG legs [39].

The output power (P) was calculated using Equation (4):

$$P = I^2 \cdot R_{load} = \left(\frac{V_{oc}}{R_{in} + R_{load}} \right)^2 \cdot R_{load} \quad (4)$$

where I , R_{load} , and R_{in} are respectively the output current, the load resistance, and the internal resistance of the homemade TEG³⁷. The R_{in} and R_{load} values were both 770 Ω , and the calculated maximum output power was 80.1 nW at $\Delta T = 30$ K.

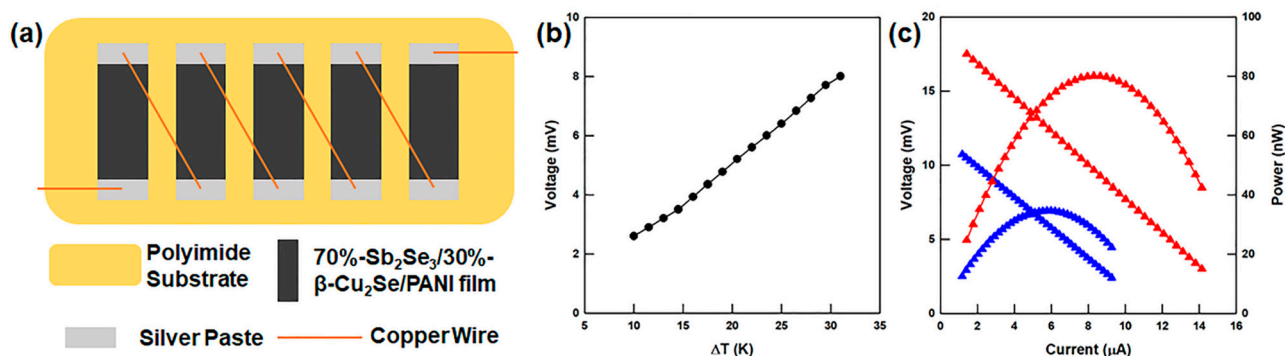


Figure 6. (a) Schematic diagram of the TEG structure, (b) open-circuit voltage at various temperature differences, and (c) output voltage and output power versus current at temperature differences at 20 K and 30 K.

4. Conclusions

Two nanowire materials, namely Sb_2Se_3 and $\beta\text{-Cu}_2\text{Se}$, were synthesized via hydrothermal reaction and water evaporation-induced self-assembly methods, respectively. The conducting polymer, PANI was then formed on the Sb_2Se_3 and $\beta\text{-Cu}_2\text{Se}$ nanowire surfaces in order to improve their electrical conductivities. Composite PANI-coated materials with various ratios of Sb_2Se_3 and $\beta\text{-Cu}_2\text{Se}$ were produced, and their thermoelectric properties were measured. The 70%- Sb_2Se_3 /30%- $\beta\text{-Cu}_2\text{Se}$ /PANI film was shown to provide the highest power factor of $181.61 \mu\text{W}/\text{m}\cdot\text{K}^2$ at 473 K. In addition, a thermoelectric generator was fabricated from five legs of the 70% Sb_2Se_3 /30% $\beta\text{-Cu}_2\text{Se}$ /PANI film and was found to provide an open-circuit voltage of 7.9 mV and an output power of 80.1 nW at $\Delta T = 30$ K. This study demonstrates that the fabricated flexible TEG which combines the high performance of inorganic thermoelectric materials with flexibility of a polymer has potential application as a next-generation power generator for wearable or portable devices. In addition, this study can also influence other electronic devices requiring compact power generators.

Supplementary Materials: The following are available online at <https://www.mdpi.com/article/10.3390/polym13091518/s1>, Figure S1: Raman spectrum of Sb_2Se_3 nanowires, Figure S2: Raman spectrum of $\beta\text{-Cu}_2\text{Se}$ nanowires, Figure S3: FE-SEM images of Sb_2Se_3 / $\beta\text{-Cu}_2\text{Se}$ nanowires before and after PANI coating on the nanowire surfaces, Figure S4: Raman spectrum of 70%- Sb_2Se_3 /30%- $\beta\text{-Cu}_2\text{Se}$ /PANI powders, Figure S5: Macro-scaled morphology of the 70%- Sb_2Se_3 /30%- $\beta\text{-Cu}_2\text{Se}$ /PANI flexible film.

Author Contributions: Conceptualization, investigation, writing—original draft, M.K.; data curation, D.P.; supervision, project administration, funding acquisition, J.K. All authors have read and agreed to the published version of the manuscript.

Funding: This research was funded and conducted under the Competency Development Program for Industry Specialists of the Korean Ministry of Trade, Industry and Energy (MOTIE), operated by Korea Institute for Advancement of Technology (KIAT). (No. P0012453, Next-generation Display Expert Training Project for Innovation Process and Equipment, Materials Engineers).

Institutional Review Board Statement: Not applicable.

Informed Consent Statement: Not applicable.

Data Availability Statement: The data presented in this study are available on the request from the corresponding author.

Conflicts of Interest: The authors declare no conflict of interest.

References

- Chen, B.; Das, S.R.; Zheng, W.; Zhu, B.; Xu, B.; Hong, S.; Sun, C.; Wang, X.; Wu, Y.; Claussen, J.C. Inkjet Printing of Single-Crystalline Bi_2Te_3 Thermoelectric Nanowire Networks. *Adv. Electron. Mater.* **2017**, *3*, 1600524. [[CrossRef](#)]
- Bao, D.; Chen, J.; Yu, Y.; Liu, W.; Huang, L.; Han, G.; Tang, J.; Zhou, D.; Yang, L.; Chen, Z.-G. Texture-dependent thermoelectric properties of nano-structured Bi_2Te_3 . *Chem. Eng. J.* **2020**, *388*, 124295. [[CrossRef](#)]

3. Han, C.; Tan, G.; Varghese, T.; Kanatzidis, M.G.; Zhang, Y. High-Performance PbTe Thermoelectric Films by Scalable and Low-Cost Printing. *ACS Energy Lett.* **2018**, *3*, 818–822. [[CrossRef](#)]
4. Chen, Z.; Jian, Z.; Li, W.; Chang, Y.; Ge, B.; Hanus, R.; Yang, J.; Chen, Y.; Huang, M.; Snyder, G.J.; et al. Lattice Dislocations Enhancing Thermoelectric PbTe in Addition to Band Convergence. *Adv. Mater.* **2017**, *29*. [[CrossRef](#)]
5. Burton, M.R.; Mehraban, S.; Beynon, D.; McGettrick, J.; Watson, T.; Lavery, N.P.; Carnie, M.J. 3D Printed SnSe Thermoelectric Generators with High Figure of Merit. *Adv. Energy Mater.* **2019**, *9*, 1900201. [[CrossRef](#)]
6. Burton, M.R.; Liu, T.; McGettrick, J.; Mehraban, S.; Baker, J.; Pockett, A.; Watson, T.; Fenwick, O.; Carnie, M.J. Thin Film Tin Selenide (SnSe) Thermoelectric Generators Exhibiting Ultralow Thermal Conductivity. *Adv. Mater.* **2018**, *30*, e1801357. [[CrossRef](#)] [[PubMed](#)]
7. Perez-Taborda, J.A.; Vera, L.; Caballero-Calero, O.; Lopez, E.O.; Romero, J.J.; Stroppa, D.G.; Briones, F.; Martin-Gonzalez, M. Pulsed Hybrid Reactive Magnetron Sputtering for High zT Cu₂Se Thermoelectric Films. *Adv. Mater. Technol.* **2017**, *2*, 1700012. [[CrossRef](#)]
8. Lei, J.; Ma, Z.; Zhang, D.; Chen, Y.; Wang, C.; Yang, X.; Cheng, Z.; Wang, Y. High thermoelectric performance in Cu₂Se superionic conductor with enhanced liquid-like behaviour by dispersing SiC. *J. Mater. Chem. A* **2019**, *7*, 7006–7014. [[CrossRef](#)]
9. Prado-Gonjal, J.; Phillips, M.; Vaqueiro, P.; Min, G.; Powell, A.V. Skutterudite Thermoelectric Modules with High Volume-Power-Density: Scalability and Reproducibility. *ACS Appl. Energy Mater.* **2018**, *1*, 6609–6618. [[CrossRef](#)]
10. Lan, S.; Yang, Z.; Stobart, R.; Chen, R. Prediction of the fuel economy potential for a skutterudite thermoelectric generator in light-duty vehicle applications. *Appl. Energy* **2018**, *231*, 68–79. [[CrossRef](#)]
11. Shuai, J.; Mao, J.; Song, S.; Zhang, Q.; Chen, G.; Ren, Z. Recent progress and future challenges on thermoelectric Zintl materials. *Mater. Today Phys.* **2017**, *1*, 74–95. [[CrossRef](#)]
12. Song, S.; Mao, J.; Bordelon, M.; He, R.; Wang, Y.; Shuai, J.; Sun, J.; Lei, X.; Ren, Z.; Chen, S.; et al. Joint effect of magnesium and yttrium on enhancing thermoelectric properties of n-type Zintl Mg_{3+δ}Y_{0.02}Sb_{1.5}Bi_{0.5}. *Mater. Today Phys.* **2019**, *8*, 25–33. [[CrossRef](#)]
13. Lu, Y.; Ding, Y.; Qiu, Y.; Cai, K.; Yao, Q.; Song, H.; Tong, L.; He, J.; Chen, L. Good Performance and Flexible PEDOT:PSS/Cu₂Se Nanowire Thermoelectric Composite Films. *ACS Appl. Mater. Interfaces* **2019**, *11*, 12819–12829. [[CrossRef](#)] [[PubMed](#)]
14. Fan, Z.; Li, P.; Du, D.; Ouyang, J. Significantly Enhanced Thermoelectric Properties of PEDOT:PSS Films through Sequential Post-Treatments with Common Acids and Bases. *Adv. Energy Mater.* **2017**, *7*, 1602116. [[CrossRef](#)]
15. Wang, X.; Kyaw, A.K.K.; Yin, C.; Wang, F.; Zhu, Q.; Tang, T.; Yee, P.I.; Xu, J. Enhancement of thermoelectric performance of PEDOT:PSS films by post-treatment with a superacid. *RSC Adv.* **2018**, *8*, 18334–18340. [[CrossRef](#)]
16. Wu, R.; Yuan, H.; Liu, C.; Lan, J.-L.; Yang, X.; Lin, Y.-H. Flexible PANI/SWCNT thermoelectric films with ultrahigh electrical conductivity. *RSC Adv.* **2018**, *8*, 26011–26019. [[CrossRef](#)]
17. Meng, C.; Liu, C.; Fan, S. A Promising Approach to Enhanced Thermoelectric Properties Using Carbon Nanotube Networks. *Adv. Mater.* **2010**, *22*, 535–539. [[CrossRef](#)]
18. Li, H.; Liu, S.; Li, P.; Yuan, D.; Zhou, X.; Sun, J.; Lu, X.; He, C. Interfacial control and carrier tuning of carbon nanotube/polyaniline composites for high thermoelectric performance. *Carbon* **2018**, *136*, 292–298. [[CrossRef](#)]
19. Zhang, J.; Song, G.; Qiu, L.; Feng, Y.; Chen, J.; Yan, J.; Liu, L.; Huang, X.; Cui, Y.; Sun, Y.; et al. Highly Conducting Polythiophene Thin Films with Less Ordered Microstructure Displaying Excellent Thermoelectric Performance. *Macromol. Rapid Commun.* **2018**, *39*, e1800283. [[CrossRef](#)] [[PubMed](#)]
20. Wang, Y.; Yang, J.; Wang, L.; Du, K.; Yin, Q.; Yin, Q. Polypyrrole/Graphene/Polyaniline Ternary Nanocomposite with High Thermoelectric Power Factor. *ACS Appl. Mater. Interfaces* **2016**, *9*, 20124–20131. [[CrossRef](#)] [[PubMed](#)]
21. Liang, L.; Chen, G.; Guo, C.-Y. Polypyrrole nanostructures and their thermoelectric performance. *Mater. Chem. Front.* **2016**, *1*, 380–386. [[CrossRef](#)]
22. Park, D.; Ju, H.; Kim, J. Enhanced thermoelectric properties of flexible N-type Ag₂Se nanowire/polyvinylidene fluoride composite films synthesized via solution mixing. *J. Ind. Eng. Chem.* **2021**, *93*, 333–338. [[CrossRef](#)]
23. Zapien, J.A.; Islam, A.K.M.F.U.; Liu, C.; Kamruzzaman, M. A comparative study on the electronic and optical properties of Sb₂Se₃ thin film. *Semicond* **2017**, *51*, 1673.
24. Jin, R.; Liu, Z.; Yang, L.; Liu, J.; Xu, Y.; Li, G. Facile synthesis of sulfur doped Sb₂Se₃ nanosheets with enhanced electrochemical performance. *J. Alloy. Compd.* **2013**, *579*, 209–217. [[CrossRef](#)]
25. Zhang, C.; Li, Z.; Guo, Y.; Niu, X.; Liang, X.; Zhou, N.; Zhu, H.; Chen, J.; Mai, Y. Controllable Synthesis and Properties of Sb₂Se₃ Nanorods Synthesized by Hot-Injection Method. *J. Nanosci. Nanotechnol.* **2017**, *17*, 1338–1344. [[CrossRef](#)] [[PubMed](#)]
26. Ko, T.-Y.; Shellaiah, M.; Sun, K.W. Thermal and Thermoelectric Transport in Highly Resistive Single Sb₂Se₃ Nanowires and Nanowire Bundles. *Sci. Rep.* **2016**, *6*, 35086. [[CrossRef](#)]
27. Yang, L.; Chen, Z.-G.; Han, G.; Hong, M.; Zou, Y.; Zou, J. High-performance thermoelectric Cu₂Se nanoplates through nanostructure engineering. *Nano Energy* **2015**, *16*, 367–374. [[CrossRef](#)]
28. Chen, X.; Li, Z.; Yang, J.; Sun, Q.; Dou, S. Aqueous preparation of surfactant-free copper selenide nanowires. *J. Colloid Interface Sci.* **2015**, *442*, 140–146. [[CrossRef](#)] [[PubMed](#)]
29. Kim, M.; Park, D.; Kim, J. Synergistically enhanced thermoelectric performance by optimizing the composite ratio between hydrothermal Sb₂Se₃ and self-assembled β-Cu₂Se nanowires. *CrystEngComm* **2021**, *23*, 2880–2888. [[CrossRef](#)]
30. Chen, M.; Gao, L. Polyol method synthesis and characterization of nanoscale Sb₂Se₃ wires. *Mater. Res. Bull.* **2005**, *40*, 1120–1125. [[CrossRef](#)]

31. Ma, Z.; Chai, S.; Feng, Q.; Li, L.; Li, X.; Huang, L.; Liu, D.; Sun, J.; Jiang, R.; Zhai, T.; et al. Chemical Vapor Deposition Growth of High Crystallinity Sb₂Se₃ Nanowire with Strong Anisotropy for Near-Infrared Photodetectors. *Small* **2019**, *15*, e1805307. [[CrossRef](#)]
32. Khan, M.D.; Aamir, M.; Sohail, M.; Sher, M.; Akhtar, J.; Malik, M.A.; Revaprasadu, N. Novel single source precursor for synthesis of Sb₂Se₃ nanorods and deposition of thin films by AACVD: Photo-electrochemical study for water reduction catalysis. *Sol. Energy* **2018**, *169*, 526–534. [[CrossRef](#)]
33. Lesnyak, V.; Brescia, R.; Messina, G.C.; Manna, L. Cu Vacancies Boost Cation Exchange Reactions in Copper Selenide Nanocrystals. *J. Am. Chem. Soc.* **2015**, *137*, 9315–9323. [[CrossRef](#)] [[PubMed](#)]
34. Padmapriya, S.; Harinipriya, S.; Jaidev, K.; Sudha, V.; Kumar, D.; Pal, S. Storage and evolution of hydrogen in acidic medium by polyaniline. *Int. J. Energy Res.* **2018**, *42*, 1196–1209. [[CrossRef](#)]
35. Babu, V.J.; Vempati, S.; Ramakrishna, S. Conducting Polyaniline-Electrical Charge Transportation. *Mater. Sci. Appl.* **2013**, *4*, 1–10. [[CrossRef](#)]
36. Patil, S.H.; Gaikwad, A.P.; Sathaye, S.D.; Patil, K.R. To form layer by layer composite film in view of its application as supercapacitor electrode by exploiting the techniques of thin films formation just around the corner. *Electrochim. Acta* **2018**, *265*, 556–568. [[CrossRef](#)]
37. Park, D.; Kim, M.; Kim, J. Conductive PEDOT: PSS-Based Organic/Inorganic Flexible Thermoelectric Films and Power Generators. *Polymer* **2021**, *13*, 210. [[CrossRef](#)]
38. Ju, H.; Park, D.; Kim, J. Thermoelectric enhancement in multilayer thin-films of tin chalcogenide nanosheets/conductive polymers. *Nanoscale* **2019**, *11*, 16114–16121. [[CrossRef](#)] [[PubMed](#)]
39. Lu, Y.; Qiu, Y.; Cai, K.; Li, X.; Gao, M.; Jiang, C.; He, J. Ultrahigh performance PEDOT/Ag₂Se/CuAgSe composite film for wearable thermoelectric power generators. *Mater. Today Phys.* **2020**, *14*, 100223. [[CrossRef](#)]